ACS APPLIED MATERIALS & INTERFACES

Research Article

www.acsami.org

Preclinical Evaluation of Antitumor Activity of Acid-Sensitive PEGylated Doxorubicin

Diankui Sun,[†] Jianxun Ding,*[,†] Chunsheng Xiao,[†] Jinjin Chen,[†,‡] Xiuli Zhuang,*[,†] and Xuesi Chen[†]

[†]Key Laboratory of Polymer Ecomaterials, Changchun Institute of Applied Chemistry, Chinese Academy of Sciences, Changchun 130022, People's Republic of China

[‡]University of Chinese Academy of Sciences, Beijing 100039, People's Republic of China

Supporting Information

ABSTRACT: The acid-sensitive PEGylated doxorubicin (DOX) with exact chemical structure was designed and prepared as a potential tumor intracellular microenvironment-responsive drug delivery system. First, the insensitive succinic anhydride-functionalized DOX (i.e., SAD) and acid-sensitive *cis*-aconitic anhydride-modified DOX (i.e., CAD) were synthesized through the ring-opening reaction. Subsequently, the insensitive and acid-sensitive PEGylated DOX (i.e., mPEG-SAD and mPEG-CAD) was prepared by the condensation reaction between the terminal hydroxyl group of mPEG and the carboxyl group in SAD and CAD, respectively. The obtained mPEG-SAD and mPEG-CAD could spontaneously self-assemble into micelles in phosphate-buffered saline at pH 7.4 with diameters of about 100 nm. The DOX release of mPEG-CAD micelle could be accelerated by the decrease of pH from 7.4, 6.8, to 5.5 in relation to that of mPEG-SAD micelle. On the other hand, the result of the cellular proliferation inhibition test indicated that mPEG-CAD micelle exhibited favorable antiproliferative activity in vitro. In addition, the selective intratumoral accumulation and antitumor efficacy of mPEG-CAD micelle were significantly better than those of free DOX and mPEG-SAD. More importantly, the prodrug micelles exhibited upregulated security in vivo as compared to free DOX. Overall, the mPEG-CAD micelle with enhanced antitumor efficacy and decreased side effects was a fascinating prospect for the clinical chemotherapy of malignancy.

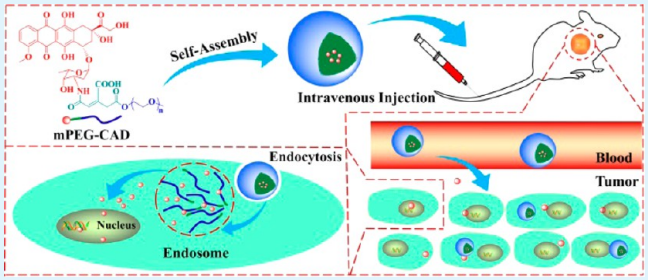

KEYWORDS: *controlled drug delivery, doxorubicin, acid-sensitive, poly(ethylene glycol), malignancy therapy*

1. INTRODUCTION

Malignancy has been one of the leading causes of human deaths all over the world.[1] Chemotherapy is the main clinical treatment approach among all traditional modalities.[2] Although chemotherapy significantly progresses,[3] some severe obstacles are still not solved, such as inadequate amount of drug reaching the lesion site and serious undesired side effects.[4] Nanotechnology has raised the expectation in malignancy treatment,[5] and is considered as one of the most promising directions.[6] Among all existing nanoscale drug delivery systems,[7] for example, liposome,[8−10] micelle,[11−13] vesicle,[5] and nanogel,[14−16] micelle develops more quickly and draws great attention. Amphiphilic block or graft copolymers could self-assemble into micelles as drug carriers.[17] The packaging ways of micelles for antitumor drugs can be divided into two types: physical encapsulation and chemical conjugation. In contrast to the physical package, chemical bonding provides a more stable loading of drug and more durable drug release, which has been more extensively researched.[18,19]

Doxorubicin (DOX), an anthracycline antibiotic, has been widely applied in clinical chemotherapy of various malignant tumors.[20] DOX interacts with DNA to inhibit the DNA replication and protein synthesis.[21] However, free DOX causes serious dose-dependent side effects in the process of chemotherapy.[18,20] As a result, the development of new formulations of DOX has been the focus of research.[22,23] Therefore, it is urgent to develop an excellent drug delivery system that can effectively transfer DOX into tumor tissue and even cells without damage to normal tissues.[24] In vivo inhibition efficacy and security to a target cell are the key factors affecting the malignancy treatments of antineoplastic agents.[20] An ideal drug delivery system exhibits intelligent "on-demand" transportation and release,[21,25] and a little or no malicious release in normal tissues.[26] In recent years, the macromolecularization of DOX has been an important approach for the development of chemotherapeutic drugs to prolong circulation in vivo, enhance cellular uptake and efficacy, and overcome the serious side effects.[20,27]

Recently, the stimuli-responsive nanovehicles have been widely exploited for controlled antitumor drug delivery, which show a sharp intelligent response to the specific internal stimuli, such as enzyme,[28,29] temperature,[30] photo,[31,32] redox,[4,33] and/

Received: September 10, 2014
Accepted: November 6, 2014
Published: November 21, 2014

Scheme 1. Schematic Illustration for Preparation of pH-Responsive mPEG-CAD Micelle and in Vivo Circulation, Accumulation in Tumor Tissue, and Final pH-Triggered Intracellular DOX Release after Intravenous Injection

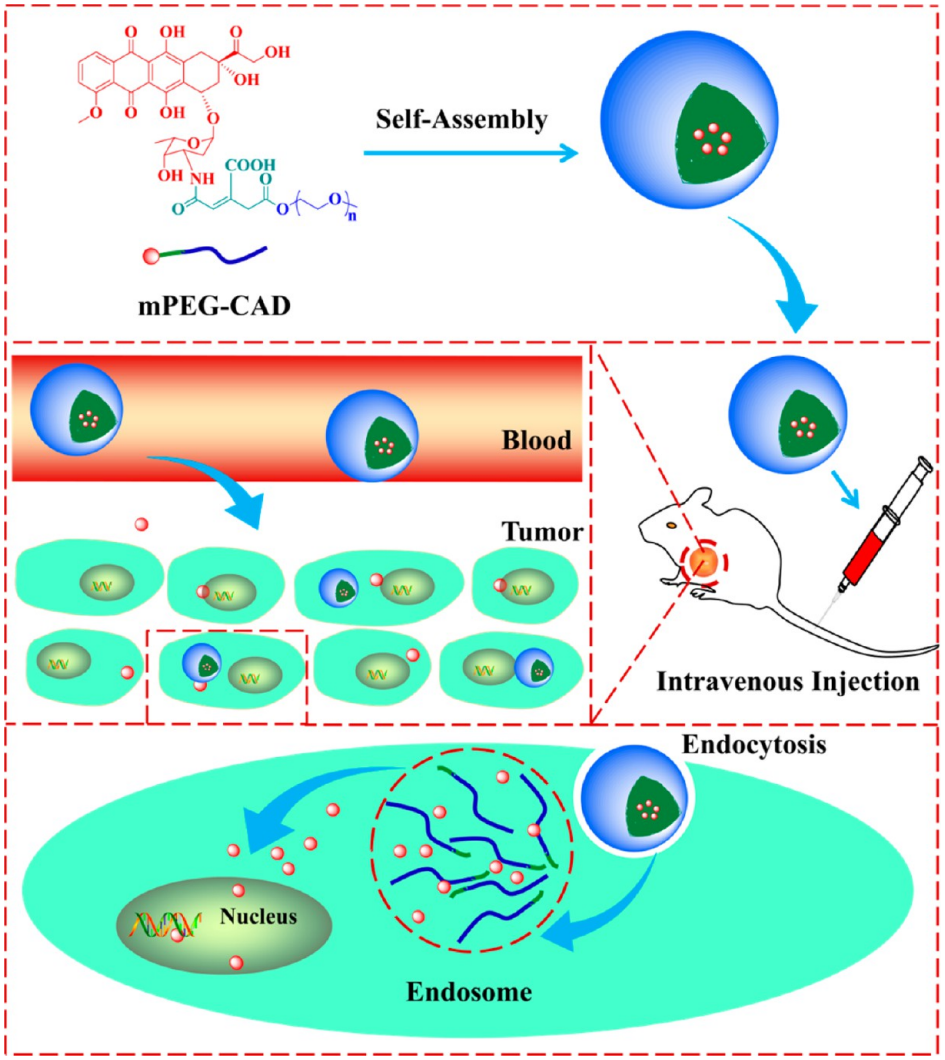

or pH.[34−36] Among them, pH-responsiveness is the most important and common, and has received great attention because of the existential pH differences between physiological condition and tumor tissue or intracellular compartments.[21] For example, the pH in normal physiological condition (~7.4) is slightly higher than that in tumor tissue (~6.8),[37,38] while the intracellular endosomal and lysosomal pH values (pH 5.0−6.5) are significantly lower than that of extracellular microenvironment.[4,21,39] Benefiting from the different pH potentials, the pH-responsive nanosystems have been the most widely developed smart platforms for controlled drug delivery in malignancy therapy.[7] So far, plenty of intelligent polymer−drug conjugates based on intracellular pH-sensitive covalent bonds,[20,22] such as hydrazone,[36,40] acetal,[41] amido,[37,42] Schiff base,[43] and orthoester bonds,[33] have been widely reported. The nanovehicles based on the above pH-responsive macromolecularized drugs possess a large number of advantages, including (1) prolonged circulation time in blood,[44] (2) enhanced accumulation in tumor tissue,[45] (3) promoted cell internalization,[4] and (4) significantly accelerated intracellular drug release[37,46] to improve the efficacy and overcome the adverse reactions. Under ideal circumstances, the packaged antitumor drugs should not be leaked during circulation in the bloodstream, while the downregulated tumor tissular or intracellular pH can be considered as an ideal trigger for "on-demand" release of antitumor drugs.[47]

In this work, through the condensation reaction between methoxy poly(ethylene glycol) (mPEG) and succinic anhydride (SA) or *cis*-aconitic anhydride (CA)-modified DOX (referred as SAD or CAD, respectively), the unresponsive mPEG-SAD and pH-responsive mPEG-CAD were separately synthesized through a facile and efficient condensation reaction (Schemes S1 and S2, Supporting Information). As depicted in Scheme 1, the obtained prodrugs self-assembled into nanoscale micelles in aqueous solutions. mPEG-CAD contained an acid-sensitive amide linker, which allowed DOX to be selectively released in the endosome or lysosome after endocytosis. As a result, the acid-sensitive mPEG-CAD micelle exhibited favorable antiproliferative activity as compared to the insensitive mPEG-SAD micelle. More importantly, mPEG-CAD micelle can significantly inhibit the tumor growth toward H22-transplanted mouse models by tail vein injection as compared to the unresponsive mPEG-SAD micelle, which benefited from the selective acidity-triggered DOX release in tumor cells. Therefore, the exploited acid-sensitive PEGylated DOX exhibited great potential for the clinical chemotherapy of malignancy.

2. MATERIALS AND METHODS

2.1. Materials. SA, CA, mPEG (M_n = 750 g mol^{-1}), 1,6-diphenyl-1,3,5-hexatriene (DPH), 3-(4.5-dimethyl-thiazol-2-yl)-2.5-diphenyl tetrazolium bromide (MTT), 4′,6-diamidino-2-phenylindole (DAPI), and Alexa Fluor 488 phalloidin (Alexa 488) were purchased from Sigma-Aldrich (Steinheim, Germany). Doxorubicin hydrochloride (DOX·HCl) was obtained from Zhejiang Hisun Pharmaceutical Co., Ltd. (Zhejiang, P. R. China). *N*,*N*-Dimethylformamide (DMF) was pretreated with calcium hydride for 72 h and subsequently distilled under reduced pressure. 1-Ethyl-(3-(dimethylamino)propyl) carbodiimide hydrochloride (EDC·HCl) and 4-*N*,*N*-dimethylaminopyridine (DMAP) were bought from GL Biochem Co., Ltd. (Shanghai, China). Terminal deoxynucleotidyl transferase-mediated dUTP nick-end labeling (TUNEL) kit was purchased from Roche Co. (Mannheim, Germany). Caspase-3 and surviving kits were purchased from Abcam (Cambridge, UK).

2.2. Syntheses of SAD and CAD. As shown in Schemes S1 and S2, Supporting Information, SAD or CAD was, respectively, synthesized through the ring-opening reaction between DOX and SA or CA with triethylamine as catalyst. For typical synthesis procedure of CAD, DOX·HCl (116.0 mg, 0.2 mmol) and CA (34.3 mg, 0.22 mmol) were dissolved in 10.0 mL of anhydrous DMF in a completely dried flask, and then 33.5 μL of triethylamine was added.[37,48] The mixture was stirred under a nitrogen environment in the dark at room temperature for 24 h. After that, the solution was mixed with 100.0 mL of cold ethyl acetate, and then the mixture was washed with cold acidic saturated sodium chloride solution (pH 2−3) and finally with normal saturated solution (pH 7.4). The organic layer was collected and dried with anhydrous sodium sulfate overnight. Desiccant was filtered out, and the filtrate was dried under vacuum at room temperature to obtain a red solid powder. SAD was synthesized with the same approach as CAD. The yields of SAD and CAD were 68.2% and 74.6%, respectively.

2.3. Syntheses of mPEG-SAD and mPEG-CAD. As shown in Schemes S1 and S2, Supporting Information, mPEG-SAD or mPEG-CAD was separately synthesized through the condensation reaction between mPEG and SAD or CAD with EDC·HCl and DMAP as condensing agent and catalyst, respectively. Briefly, for the synthesis of SAD and CAD, mPEG (75.0 mg, 0.1 mmol) was dissolved in dimethyl sulfoxide (DMSO), and then CAD (81.8 mg, 0.12 mmol), EDC·HCl (57.5 mg, 0.3 mmol), and DMAP (1.2 mg, 0.01 mmol) were added to the solution. The mixture was reacted in the dark at room temperature for 72 h. After that, mPEG-CAD was obtained through a dialysis method (molecular weight cutoff (MWCO) = 3500 Da) against deionized water for 48 h. mPEG-SAD was synthesized with the same approach as mPEG-CAD.

2.4. Measurements. Proton nuclear magnetic resonance (^{1}H NMR) spectra were recorded on a Bruker AV 400 NMR spectrometer operating with deuterated DMSO (DMSO-d_6) as a solvent. Fourier-transform infrared (FT-IR) spectra were recorded on a Bio-Rad Win-IR instrument using potassium bromide method. The micelles were prepared by direct dissolution method in phosphate-buffered saline (PBS) at pH 7.4. The hydrodynamic diameters (D_hs) of micelles were measured by dynamic light scattering (DLS) at 25 °C on a WyattQELS apparatus. Transmission electron microscopy (TEM) measurements were performed using a JEOL JEW-1011 with an accelerating voltage of 100 kV. The samples were prepared by dropping 10.0 μL of micelle solution (0.1 mg mL^{-1}) onto a copper grid and drying at room temperature in the air. The critical micelle concentrations (CMCs) of mPEG-CAD and mPEG-SAD micelles were detected using ultraviolet−visible absorption spectroscopy in the range of 320−400 nm. In practice, 20.0 μL of DPH in methanol (0.4 mM) was added to 2.0 mL of mPEG-SAD and mPEG-CAD micelles in PBS with various concentrations.

2.5. In Vitro DOX Release. In vitro release profiles of prodrug micelles were assessed in PBS at pH 7.4 (a mimicking normal physiological condition), 6.8 (a tumor tissular acidic microenvironment), and 5.5 (an intracellular acidic microenvironment). 1.0 mg of mPEG-SAD or mPEG-CAD micelle was dissolved in 10.0 mL of PBS and subsequently transferred into a dialysis bag (MWCO = 3500 Da), and then covered in 100.0 mL of PBS at 37 °C with continuous shaking of 70 rpm. At the fixed time intervals, 2.0 mL of release medium was taken out, and an equal volume of fresh PBS was returned to the system. The accumulative amount of released DOX was detected by fluorescence spectroscopy on a Photon Technology International Fluorescence Master System with software Felix 4.1.0 (Lawrenceville, NJ, λ_{ex} = 480 nm).

2.6. Intracellular DOX Release Analyses. The cellular uptakes of prodrug micelles and intracellular DOX release toward HepG2 cells were detected by both confocal laser scanning microscopy (CLSM) and flow cytometry (FCM).

2.6.1. CLSM. The cells were seeded on presterilized glass sheets in 6-well plates at a density of 2.0 × 10^5 cells per well in 2.0 mL of complete high glucose Dulbecco's modified Eagle's medium (HG-DMEM), and incubated at 37 °C for 24 h in 5% (v/v) carbon dioxide (CO_2). The culture medium was then replaced with a fresh one. Free DOX, or mPEG-SAD or mPEG-CAD micelle was added to each well with a DOX dosage of 5.0 μg mL^{-1}. The cells were further incubated for another 2 or 24 h. Subsequently, the cells on glass sheets were washed with PBS five times and immobilization by 4% (w/v) PBS-buffered paraformaldehyde for 20 min at room temperature. The cells then were washed with PBS five times, and treated with 0.1% (v/v) Triton 100-X in PBS for 12 min at room temperature. Finally, the cells were stained with DAPI to cell nuclei for 5 min and Alexa 488 to cell cytoskeleton for 30 min at 37 °C, and subsequently washed with PBS five times. The CLSM microimages of cells were obtained through a CLSM (LSM 780, Carl Zeiss, Jena, Germany).

2.6.2. FCM. The cellular uptake determinations were quantitatively implemented by FCM. Briefly, the cells were seeded in 6-well plates at a density of 2.0 × 10^5 cells per well in 2.0 mL of complete HG-DMEM, and incubated for 24 h at 37 °C in 5% (v/v) CO_2. The culture medium was replaced with fresh one. Free DOX, or mPEG-SAD or mPEG-CAD micelle was then added to each well with a DOX concentration at 5.0 μg mL^{-1}. The cells were cultured for another 2 or 24 h. Cells without treatment were used as control. After that, the culture medium was removed, and the cells were washed three times with PBS and then digested with trypsin. Subsequently, 1.0 mL of PBS was added to each well, and the suspended cells were centrifuged twice for 5 min at 3500 rpm. After the supernatants were removed, the cells were resuspended in 0.3 mL of PBS. Data were analyzed by CFM (Beckman, CA).

2.7. Cytotoxicity Assays. The cytotoxicities of prodrug micelles were examined with a MTT assay toward HepG2 cells (a human hepatoma cell line). The cells were seeded in 96-well plates at 8.0 × 10^3 cells per well in 180.0 μL of complete HG-DMEM, and then incubated at 37 °C in 5% (v/v) CO_2 for 24 h. Subsequently, free DOX, or mPEG-SAD or mPEG-CAD micelle was added to each well with a DOX concentration from 0−10.0 μg mL^{-1}. After incubation for another 72 h, 20.0 μL of MTT (5.0 mg mL^{-1}) was added to each well and incubated for 4 h. The upper solution was then carefully removed, and 180 μL of DMSO was added to each well to dissolve the MTT formazan crystals. The plates were shaken for 5 min before detection. The absorbances of media were measured on a Bio-Rad 680 microplate reader at 490 nm. The cell viability was calculated on the basis of eq 1:

$$\text{cell viability (\%)} = \frac{A_{\text{sample}}}{A_{\text{control}}} \times 100 \quad (1)$$

In eq 1, A_{sample} and A_{control} represent the absorbances of sample and control wells, respectively.

2.8. Hemolysis Activity Tests. Hemolytic activity properties of free DOX, and mPEG-SAD and mPEG-CAD micelles were evaluated by a spectrophotometry technique. Typically, fresh rabbit blood obtained from the Experimental Animal Center of Jilin University was stabilized with dipotassium ethylene diamine tetraacetate in normal saline (NS). Red blood cells (RBCs) were separated from the blood by centrifugation at 1500 *g* for 10 min, and then carefully washed and diluted. The suspended RBCs were cocultured with free DOX, and

mPEG-SAD and mPEG-CAD micelles of different concentrations at 37 °C for 2 h. NS and Triton X-100 (a lysing agent of RBCs) were used as negative and positive controls, respectively. After that, RBCs were separated by centrifugation at 3000 rpm for 10 min, and then 180.0 μL of the supernatant of each sample was collected and added to a 96-well plate. Free hemoglobin in the supernatant was measured with a Bio-Rad 680 microplate reader at 570 nm. The hemolytic ratio of RBCs was calculated on the basis of eq 2:

$$\text{hemolytic ratio (\%)} = \frac{A_{\text{sample}} - A_{\text{negative control}}}{A_{\text{positive control}} - A_{\text{negative control}}} \times 100 \quad (2)$$

In eq 2, A_{sample}, $A_{\text{negative control}}$, and $A_{\text{positive control}}$ were denoted as the absorbances of sample, and negative and positive controls, respectively.

2.9. Tissue Distribution Assessments. The tissue distributions of DOX after intravenous injections of various formulations were qualitatively or semiquantitatively assessed by ex vivo DOX fluorescence imaging of major internal organs. Typically, the tumor bearing mice were prepared by inoculating 3.0×10^6 H22 cells (a mouse hepatoma cell line) into Kunming mice, which were obtained from the Experimental Animal Center of Jilin University. All mice in this work were handled under the protocol approved by the Institutional Animal Care and Use Committee of Jilin University, and all efforts were made to minimize suffering. When the tumor volume increased to about 200 mm^3, free DOX, or mPEG-SAD or mPEG-CAD micelle with a dose of 5.0 mg kg^{-1} body weight on a DOX basis was injected intravenously though tail vain. The mice were sacrificed at 6 or 12 h postinjection, and the major organs including heart, liver, spleen, lung, kidney, and tumor were excised and washed with NS. The ex vivo DOX fluorescence imaging was obtained using the Maestro in vivo imaging system (Cambridge Research & Instrumentation Inc., Woburn, MA). In addition, the average signals were also semiquantitatively analyzed using a Maestro 2.4 software from the same company.

2.10. In Vivo Antitumor Assays. In vivo antitumor efficacies of free DOX, and mPEG-SAD and mPEG-CAD micelles were evaluated using the hepatoma-xenografted Kunming mice. Similarly to the detections of tissue distributions, 0.1 mL of cell suspension containing 3.0×10^6 H22 cells in PBS was injected subcutaneously into the armpits of right anterior limbs of 4−5 weeks old mice weighing from 22 to 23 g. When the tumor volume increased to about 150 mm^3, the mice were treated with NS, free DOX, or mPEG-SAD or mPEG-CAD micelle at a DOX concentration of 5.0 mg kg^{-1} body weight by the tail-veil injections on 1, 6, 11, 16, and 21 days. In the course of treatment, tumor volumes and body weights were monitored every other day. The tumor volume was calculated using eq 3:

$$V\ (\text{mm}^3) = \frac{L \times S^2}{2} \quad (3)$$

In eq 3, L and S (mm) were the largest and smallest diameters of the tumor, respectively.

2.11. Histopathological Analyses. The mice were sacrificed by cervical dislocation at 4 days after the last treatment. Tumors and major organs (i.e., heart, liver, spleen, lung, and kidney) were collected and fixed in 4% (w/v) PBS-buffered paraformaldehyde overnight and finally embedded in paraffin. The paraffin-embedded tumor and organ tissues were cut to a thickness of 5 μm, stained with hematoxylin and eosin (H&E). The histological alterations were detected by a microscope (Nikon Eclipse Ti, Optical Apparatus Co., Ardmore, PA). The relative necrotic area (%) of tumor tissue section after treatment was calculated by eq 4:

$$\text{relative necrotic area (\%)} = \frac{\text{necrotic area in tumor section}}{\text{total area in tumor section}} \times 100 \quad (4)$$

2.12. In Situ Cell Apoptosis Assays. To detect the cell apoptosis in ex vivo tumor tissues, a TUNEL assay was performed with a commercial kit following the manufacturer's instructions (Roche, Mannheim, Germany). The fluorescence microimages of tumor tissue sections were obtained through a CLSM.

2.13. Immunohistochemical Detections. Immunohistochemical detections were carried out to determine the expression of survivin and caspase-3 in ex vivo tumor tissues. For active caspase-3 detection, immunohistochemical staining was performed with antibodies against cleaved caspase-3. In addition, an optimized immunohistochemical procedure for the detection of survivin was developed by antigen retrieval methods.

2.14. Organ Damage Assays. Tissue damage indicators were performed by the corresponding functional enzymes that were detected with commercial enzyme-linked immunosorbent assay (ELISA) kits (Shanghai Lichen Biotechnology Co., Ltd., Shanghai, P. R. China). In the fourth day after the last treatment, the blood of each mouse was collected by enucleation manner into a coagulation promoting tube. After that, the blood was centrifuged at 3000 rpm for 5 min, and then the supernatant serum was collected. The clinical parameters, including heart indices containing creatine kinase (CK), creatine kinase-MB (CK-MB), and lactate dehydrogenase (LDH), liver-related alanine aminotransferase (ALT) and aspartate aminotransferase (AST), and kidney-associated blood urea nitrogen (BUN) and creatinine (Cr), were detected by the corresponding ELISA kits according to the standard protocols provided by the suppliers.

2.15. Statistical Analysis. All tests were carried out independently at least three times, and the data were expressed as mean ± standard deviation (SD). Data were analyzed for statistical significance using SPSS (Version 13.0, SPSS Inc., Chicago, IL). $p < 0.05$ was considered statistically significant, and $p < 0.01$ and $p < 0.001$ were considered highly significant.

3. RESULTS AND DISCUSSION

3.1. Syntheses and Characterizations of PEGylated DOX. As shown in Schemes S1 and S2, Supporting Information, the unresponsive mPEG-SAD and pH-responsive mPEG-CAD were accurately synthesized by the sequential ring-opening and condensation reactions. First, SAD or CAD was synthesized through the ring-opening reaction between DOX and SA or CA with triethylamine as catalyst, respectively. Second, mPEG-SAD or mPEG-CAD was obtained through the condensation reaction between mPEG and respective SAD or CAD with EDC·HCl and DMAP as condensing agent and catalyst, respectively.

The chemical structures of resulting products were confirmed by ^{1}H NMR and FT-IR spectra. As shown in Figure 1A, the peaks that appeared at 2.32 ppm (d; −C(O)CH_2CH_2C(O)−) and 2.52 ppm (e; −C(O)CH_2CH_2C(O)−) were assigned to the methylene protons in SAD. The peak at 6.05 ppm (f) belonged to the methylidyne protons in CAD (−C(O)CH═C(C(O))CH_2−), and the signal at 3.35 ppm (g) was attributed to methylene protons in CAD (−CH_2C(O)−). The peaks at 3.50 ppm (h; −CH_2C(O)−) and 3.23 ppm (i; CH_3−) were assigned to the methylene and methyl protons in PEG. The appearance of peaks at 7.93 ppm (a and b) and 7.65 ppm (c) indicated the successful conjugation of SAD or CAD to mPEG. The successful syntheses of these compounds were also confirmed by FT-IR spectra as shown in Figure 1B. The signals that appeared at 1660 cm^{-1} ($\nu_{C=O}$) and 1547 cm^{-1} ($\nu_{-CO-NH-}$) marked by a dotted line in both SAD and CAD were assigned to the stretching vibrations of amide bond. In addition to the above two signals, the characteristic peak at 1075 cm^{-1} (ν_{C-O-C}) marked by a dotted line was attributed to the stretching vibration of the ether bond of mPEG. The above results confirmed the chemical structures of both mPEG-SAD and mPEG-CAD.

The amphiphilic mPEG-SAD and mPEG-CAD could spontaneously self-assemble in aqueous solution, and the

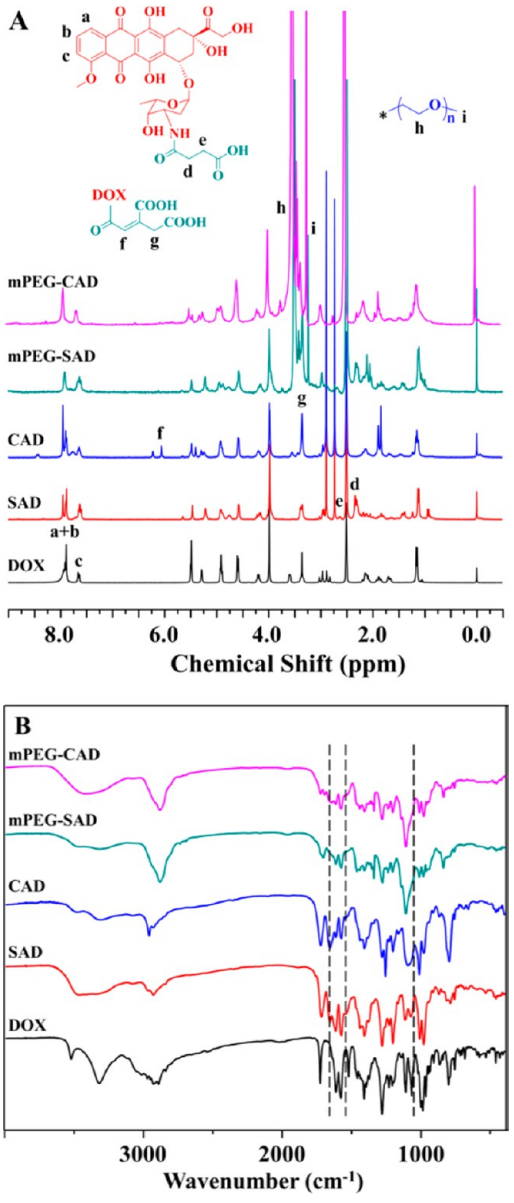

Figure 1. ^{1}H NMR (A, in DMSO-d_6) and FT-IR spectra (B) of DOX, SAD, CAD, mPEG-SAD, and mPEG-CAD.

micelles were prepared by a direct dissolution method. As shown in Figure 2, the TEM micrographs revealed that both mPEG-SAD and mPEG-CAD micelles showed clear spherical morphologies. The apparent mean diameters of mPEG-SAD and mPEG-CAD micelles from TEM measurements were detected to be about 95 and 85 nm, respectively. In comparison, the D_hs of the above two prodrug micelles tested by DLS were 119 ± 5.8 and 101 ± 6.5 nm, respectively. It was normal that the size measured by DLS was higher than that from TEM because of the swelling of micelle in aqueous environment for DLS detection.[21] The appropriate diameters of prodrug micelles (~100 nm) gave them an excellent capability to selectively accumulate in tumor region through the enhanced permeability and retention (EPR) effect.[49]

As depicted in Figure 2E, the CMCs of mPEG-SAD and mPEG-CAD micelles were determined relying on the increase of the maximum absorption intensity of DPH at 356 nm as exaltation of prodrug concentration. In detail, the CMC was calculated from the first inflection point in the sigmoidal curve

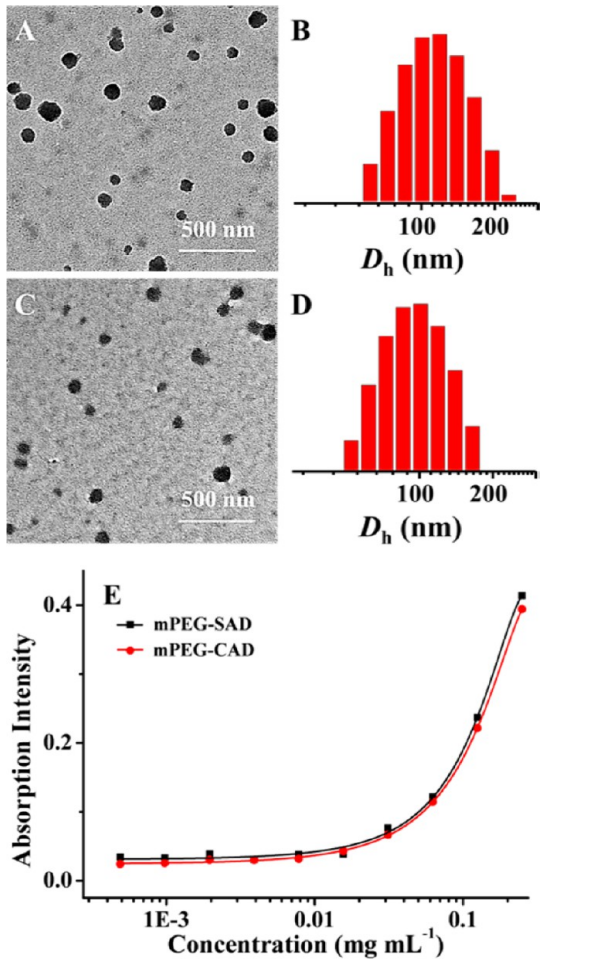

Figure 2. Typical TEM (A and C) and D_hs (B and D) of mPEG-SAD (A and B) and mPEG-CAD micelles (C and D). The maximum absorption intensities of DPH as a function of the concentrations of prodrugs (E).

of absorption intensity versus concentration. The CMC values of mPEG-SAD and mPEG-CAD micelles were calculated to be 5.3×10^{-2} and 6.0×10^{-2} mg mL^{-1}, respectively.

3.2. In Vitro DOX Release and Cellular Proliferation Inhibition. To reveal the release behaviors of mPEG-SAD and mPEG-CAD micelles, and simultaneously demonstrate the pH-sensitivity of mPEG-CAD micelle, the in vitro DOX release profiles were assessed in PBS at pH 7.4, 6.8, and 5.5, mimicking the conditions in normal physiological tissues, tumor tissular, and intracellular microenvironment, respectively. As shown in Figure 3, no significant burst release was observed from both mPEG-SAD and mPEG-CAD micelles, and only less than 17.3% and 45.5% of loaded DOX was released at pH 7.4, respectively, which indicated the prolonged blood circulation time with little leakage of drug. With the decrease of pH from 7.4 to 6.8 and even 5.5, the cumulative DOX release of mPEG-CAD was accelerated significantly up to above 58% and 98%, respectively, while those of mPEG-SAD micelle were only 15% at both pH 6.8 and 5.5. The burst release at pH 5.5 of mPEG-CAD micelle should be due to the quick breaking of the acid-sensitive linkage under acidic environment.[37] The stimuli-responsive profile of mPEG-CAD micelle could minimize the loss of drug in the circulation and enhance the release of payload in the lesion site to enhance the overall therapeutic efficacy and reduce the side effects in vivo.[21]

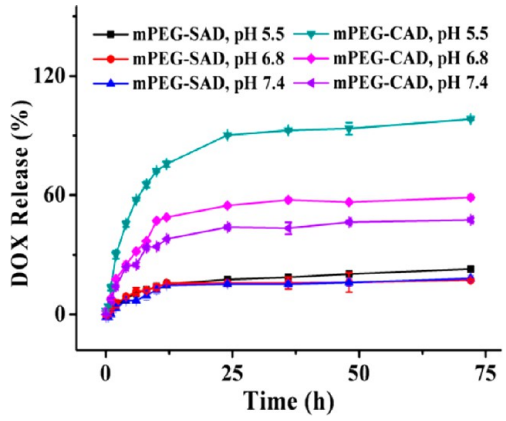

Figure 3. Release profiles of mPEG-SAD and mPEG-CAD micelles in PBS at pH 5.5, 6.8, or 7.4, 37 °C. Data were presented as a mean ± SD (n = 3).

To explore the feasibilities of prodrug micelles for intracellular drug delivery in malignancy therapy, the cellular uptakes and intracellular release behaviors of mPEG-SAD and mPEG-CAD were evaluated by CLSM and FCM toward HepG2 cells. As shown in Figure 4A, the cells cocultured with free DOX exhibited significantly higher fluorescence intensity as compared to those incubated with mPEG-SAD or mPEG-CAD micelle for 2 h, because the cellular uptakes were performed via different pathways, that is, free DOX by diffusion and prodrug micelles by endocytosis.[50] In addition, some studies have pointed out that the equivalent free DOX fluorescence was stronger than that of the loaded DOX in nanoparticles attributed to the self-quenching effect of DOX.[49,51,52] Interestingly, after incubation for 24 h, mPEG-CAD micelle-treated cells exhibited the most significant fluorescence intensity in nuclei (Figure 4B). This phenomenon could be explained by the quick cleavage of amide bond in mPEG-CAD under the acidic intracellular microenvironment. In contrast, the cells incubated with mPEG-SAD micelle exhibited extremely weak fluorescence intensity. It was because only a small amount of DOX was released into the cytoplasm and subsequently entered into the nuclei attributed to the stable amide linker in acid-insensitive mPEG-SAD. The results corresponded to the previous in vitro release behaviors in PBS.

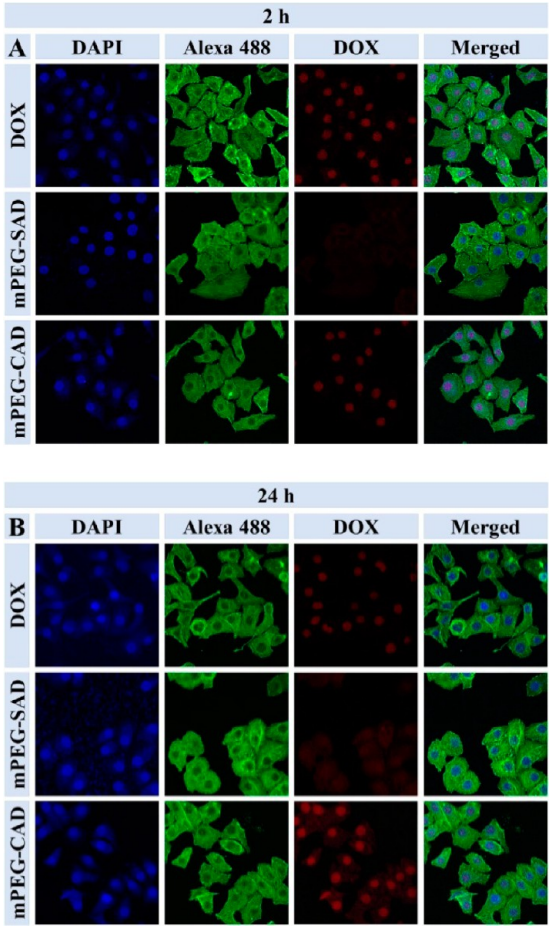

Figure 4. Representative CLSM microimages of HepG2 cells after incubation with free DOX, or mPEG-SAD or mPEG-CAD micelles for 2 (A) or 24 h (B).

For further confirmation, the cellular internalization behaviors of free DOX, and mPEG-SAD and mPEG-CAD micelles toward HepG2 cells, were analyzed by FCM. As shown in Figure 5A, the signal intensity of mPEG-CAD in the cells was significantly higher than that of mPEG-SAD at 2 h, while free DOX exhibited the highest fluorescence intensity. As shown in Figure 5B, the fluorescence intensity in the cells treated with mPEG-CAD micelle increased significantly at 24 h. However, there was no obvious change of that in mPEG-SAD micelle-treated ones. It should be attributed to the efficient endocytosis and quick DOX release induced by the intracellular acidic microenvironment-triggered cleavage of amide bond in mPEG-CAD. The FCM fluorescence intensities were statistically shown in Figure 5C in an order of mPEG-SAD < mPEG-CAD < free DOX at 2 h. The cells in free DOX groups displayed ~4.2 and 1.2 times fluorescence intensity than those of mPEG-SAD and mPEG-CAD groups, respectively. When the incubation time was prolonged to 24 h, there was a marked change in fluorescence intensity, which was in the order of mPEG-SAD < free DOX < mPEG-CAD. The DOX fluorescence intensity in the cells of mPEG-CAD group was about 1.5 and 3.0 times higher than those of free DOX and mPEG-SAD micelle in the same experiment conditions. All of the FCM results were consistent with those of the CLSM. Therefore, the enhanced DOX accumulation in the mPEG-CAD micelle-treated cells should be attributed to the efficient endocytosis and rapid intracellular DOX release.[50]

The in vitro cellular proliferation inhibitions of free DOX, and mPEG-SAD and mPEG-CAD micelles against HepG2 cells in complete HG-DMEM, were evaluated by a MTT assay. As shown in Figure 6, mPEG-CAD micelle exhibited more significant proliferation inhibition effects on HepG2 cells than that of acid-insensitive mPEG-SAD micelle at equivalent DOX concentration after incubation for 72 h, which should have resulted from the quick release of DOX at acid intracellular microenvironment.[4] More interestingly, mPEG-CAD micelle revealed higher antiproliferation efficacy even than that of free DOX. It might be because free DOX could easily diffuse across the cell membrane, while mPEG-CAD micelle was internalized through the endocytic pathway, which resulted in the greater cellular uptake and higher cytotoxic efficiency.[53] On the other hand, mPEG-SAD appeared to have a significantly lower proliferation inhibitory efficacy than free DOX due to its high stability. The quantitative analyses of antiproliferative activities of free DOX, and mPEG-SAD and mPEG-CAD micelles, were evaluated by the half-maximal inhibitory concentration (IC_{50}).

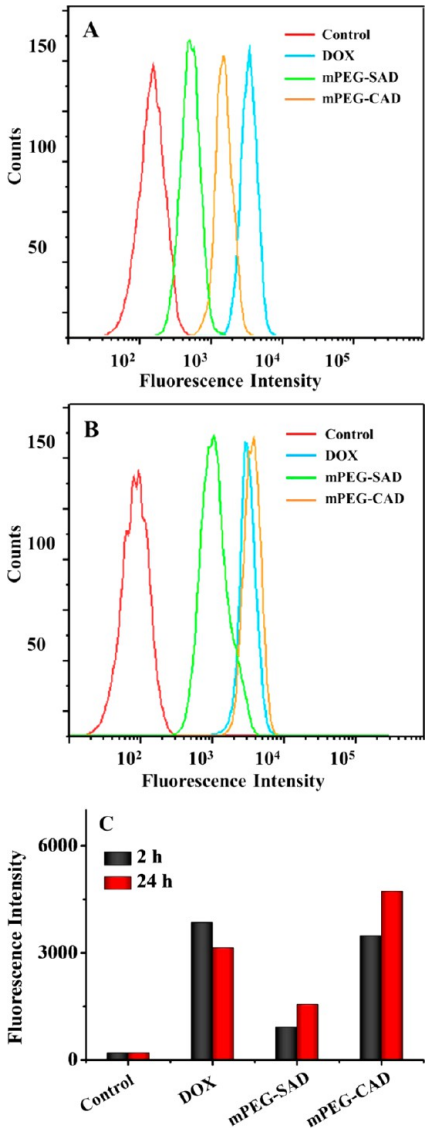

Figure 5. FCM histogram (A and B) and fluorescence intensity (C) of HepG2 cells after incubation with free DOX, or mPEG-SAD or mPEG-CAD micelle for 2 (A) or 24 h (B).

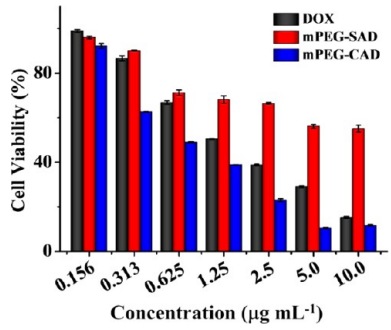

Figure 6. Cytotoxicities of free DOX, and mPEG-SAD and mPEG-CAD micelles toward HepG2 cells after coculture for 72 h. Data were presented as a mean ± SD (n = 3).

According to the calculations, mPEG-CAD micelle exhibited the lowest IC_{50} (i.e., 1.1 μg mL^{-1}) as compared to free DOX (i.e., 2.9 μg mL^{-1}) and mPEG-SAD (i.e., 16.6 μg mL^{-1}), respectively. It quantificationally confirmed that mPEG-CAD micelle exhibited an excellent inhibition effect against tumor cells relative to free DOX and mPEG-SAD micelle.

3.3. In Vivo Stability, Hemocompatibility, and Tissue Distribution. The serum-tolerance stability and hemocompatibility characterizations of prodrug micelles are important because the corresponding formulations are designed to be finally administrated via intravenous injection for most drug delivery applications.[30] In this work, the serum-tolerance stability of prodrug micelles were evaluated by determining the D_hs in 10% (v/v) serum/PBS solution through DLS. As shown in Figure S1, Supporting Information, no remarkable size change of mPEG-CAD micelle was discovered at all of the test time intervals, that is, 1, 2, 6, 12, and 24 h. The result proved that the prodrug micelles might exhibit excellent stability in blood circulation. In addition, the hemolytic activities of free DOX, and mPEG-SAD and mPEG-CAD micelles were assessed by a spectrophotometry approach. As shown in Figure S2, Supporting Information, mPEG-SAD and mPEG-CAD micelles showed almost no hemolysis at relatively high DOX concentrations up to 100.0 μg mL^{-1}, which was slightly better than that of free DOX. The results proved that the prodrug micelles exhibited excellent blood compatibility.

The tissue distribution of DOX in vivo was qualitatively detected by the fluorescence imaging of isolated major internal organs and tumors, and semiquantitatively analyzed by MaestroTM 2.4 software. As shown in Figure 7A, as compared to both free DOX and mPEG-SAD micelle, mPEG-CAD micelle accumulated at the tumor tissue site most obviously at both 6 and 12 h postinjection (p < 0.001). Moreover, both prodrug micelles exhibited less of a stay in normal organs with respect to free DOX. The results demonstrated that the pH-responsive mPEG-CAD micelle could accumulate at tumor tissues by the EPR effect. The fluorescence intensity of free DOX group was stronger than those of mPEG-SAD and mPEG-CAD micelle groups in liver and kidney, which attributed that free DOX was mainly captured and metabolized by liver and kidney. In addition, mPEG-SAD micelle appeared to have a significantly lower fluorescence intensity than mPEG-CAD micelle in all of the test organs and tumors due to its high stability.

The semiquantitative fluorescence intensity of DOX distributed in organs and tumors at 6 and 12 h after injection was also analyzed and displayed in Figure 7B. The results showed that the fluorescence intensity of mPEG-CAD micelle group in the tumor tissue was 2.1- and 7.8-fold higher than that of free DOX and mPEG-SAD micelle groups, respectively. On the other hand, the accumulation of mPEG-CAD and mPEG-SAD micelles remarkably reduced to 50% and 83% in heart, and to 38% and 66% in kidney as compared to free DOX, respectively. Similar results were also discovered at 12 h postinjection. Hence, all of the above results showed that the prodrug micelles, especially mPEG-CAD, could significantly selectively accumulate at tumors instead of internal organs as compared to free DOX.

3.4. In Vivo Tumor Suppression. To illustrate the advantages of prodrug micelles for in vivo malignancy treatment, the antitumor efficacies toward female Kunming mice bearing hepatoma tumors were studied. The treatment proposals included four groups: NS, free DOX, and mPEG-SAD and mPEG-CAD micelles, which were all administrated by intravenous injection.

The changes of tumor volumes were monitored in the course of treatment and shown in Figure 8A. The tumor volume of NS

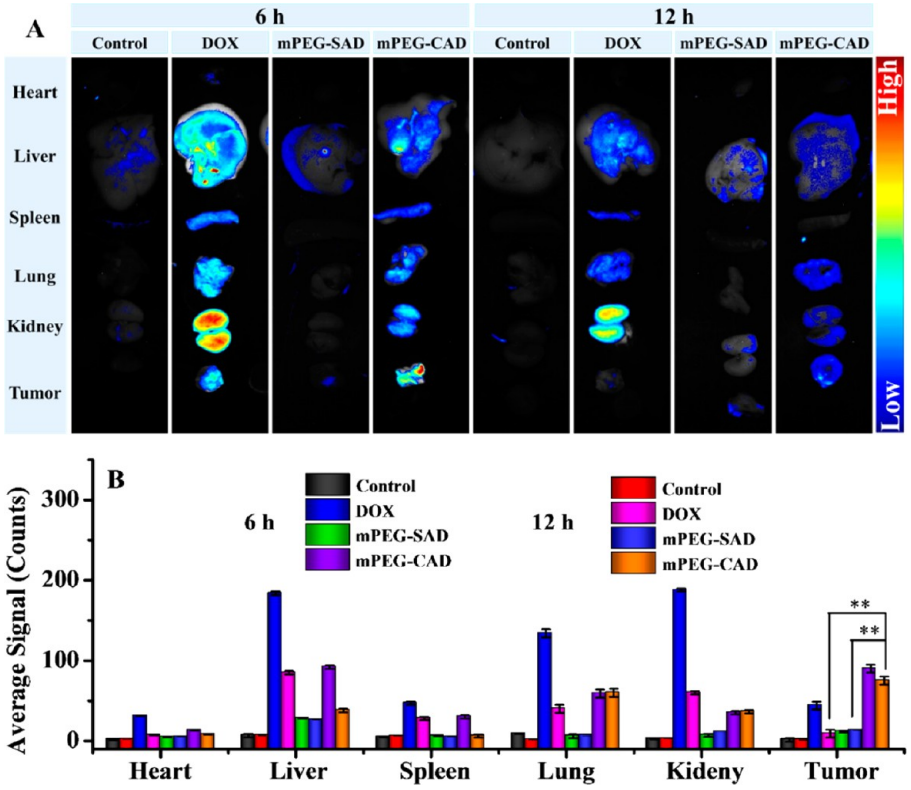

Figure 7. Ex vivo DOX fluorescence images (A) and semiquantitatively analyzed average fluorescence intensities (B) of major visceral organs (i.e., heart, liver, spleen, lung, and kidney) and tumors isolated at 6 or 12 h postinjection of NS, DOX, or mPEG-SAD or mPEG-CAD micelle in Kunming mice bearing H22 tumors. Statistical data were presented as a mean ± SD (n = 3, $^{**}p < 0.001$).

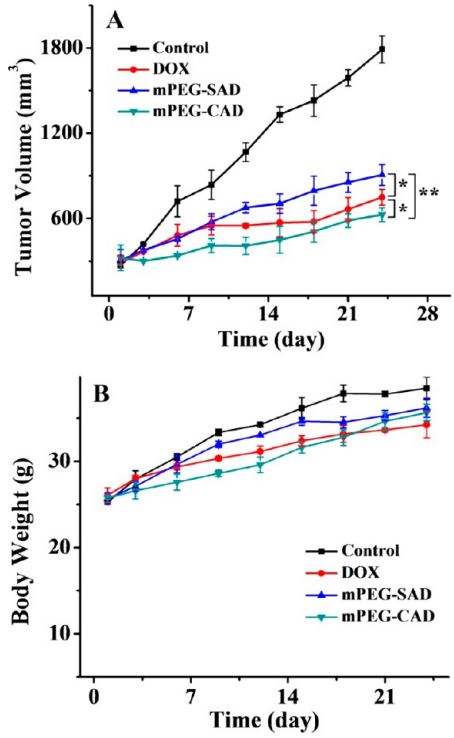

Figure 8. Tumor volume (A) and body weight evolutions (B) of H22-xenografted Kunming mice (female) after treatment with free DOX, or mPEG-SAD or mPEG-CAD micelle employed NS as control. Data were presented as a mean ± SD (n = 10; $^{*}p < 0.05$, $^{**}p < 0.001$).

group increased rapidly, while all DOX formulation-treated groups, including free DOX, the mPEG-SAD and mPEG-CAD micelles, had a significant tumor inhibition effect. On day 24 after the last treatment, the average tumor volumes of free DOX, and mPEG-SAD and mPEG-CAD micelle groups were 41.8%, 50.3%, and 35.0% of that of NS group, respectively ($p <$ 0.001). The tumor inhibition efficacy of mPEG-CAD micelle was obviously higher than that of mPEG-SAD micelle ($p <$ 0.001), which resulted from its enhanced micelle accumulation at tumor tissue and improved DOX release in tumor cells due to the EPR effect and acidic intracellular microenvironment, respectively. On the other hand, as compared to free DOX, mPEG-CAD group also revealed a more obvious tumor inhibition effect ($p < 0.05$). The lower antitumor efficacy of free DOX should be attributed to the quick excretion by glomerular filtration.[21]

To further evaluate the antitumor efficacies of the above formulations, the histopathological analyses of tumor tissues were carried out. In H&E staining, as shown in Figure 9, the nuclei were stained blue purple by hematoxylin, while the cytoplasm and extracellular matrix were dyed pink by eosin. It was obvious that the nucleus size of tumor cell was different, and the shape was irregular from each other in the NS group. Moreover, the tumor cell in this group had clear cellular morphology and chromatin. These results showed that the tumor cells were in rapid growth. In addition, a small quantity of nuclear shrinkage and fragmentation was observed in the mPEG-SAD micelle group, which indicated a low degree of tumor cell necrosis. In contrast, various greater degrees of tumor cell necrosis, tumor cell nucleus contraction, crush, and even disappearance were observed in both free DOX and mPEG-CAD micelle groups. More interestingly, the tumor

dx.doi.org/10.1021/am506178c | ACS Appl. Mater. Interfaces 2014, 6, 21202−21214

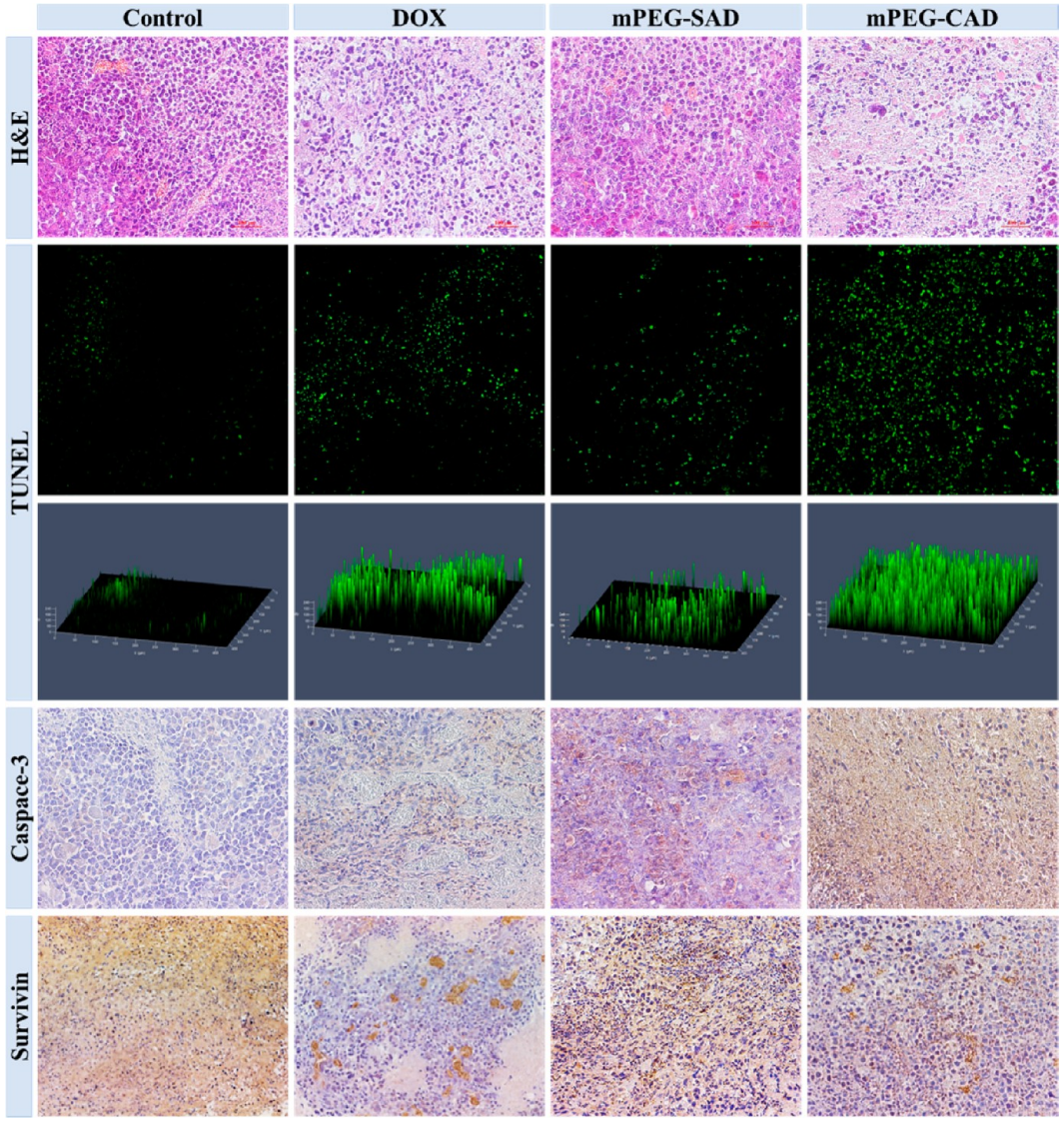

Figure 9. Ex vivo histopathological (i.e., H&E), in situ cell apoptosis (i.e., TUNEL), and immunohistochemical analyses (i.e., caspace-3 and survivin) of H22 tumor sections after treatment with NS, free DOX, or mPEG-SAD or mPEG-CAD micelle. Magnification: 200×.

tissue of mPEG-CAD group exhibited the largest necrosis areas among all of the groups. In particular, as shown in Figure S3, Supporting Information, the relative necrosis areas of free DOX, and mPEG-SAD and mPEG-CAD micelles, were ~4.1, 2.4, and 7.3 times larger than that of NS group ($p < 0.001$), respectively.

To validate in situ tumor cell apoptosis, the TUNEL evaluations were carried out. As shown in Figure 9, the DNA fragmentations in the nuclei, a marker of late apoptosis, were stained as green by a fluorescent probe. The fluorescent intensity of the mPEG-CAD micelle-treated tumor was the strongest among all of the experiment groups, which was consistent with the efficient capability of antitumor in vivo and histopathological results.

Interleukin 1β-converting enzyme-like proteases caspases are the crucial components of cell death pathways.[54] Caspase-3 is commonly activated by the numerous deaths signals and cleaves a variety of important cellular proteins. At the start of cell apoptosis, the most commonly activated caspase-3 can mediate the limited proteolysis of these proteins, as well as induce the cleavage inactivation of DNA fragmentation. As shown in Figure 9, caspase-3 was analyzed in the tumor sections by immunohistochemistry. The intensive positive signal was upregulated in the mPEG-CAD micelle-treated tumor tissue section as compared to that in free DOX and mPEG-SAD micelle groups, indicating that more cells underwent apoptosis. The results showed that mPEG-CAD micelle had more significant cell apoptosis.

Survivin is a 16.5 kDa protein, which belongs to the inhibitors of apoptosis proteins. It has been found to be expressed in the G2/M phase of the cell cycle in almost exclusive tumor cells, while it is absent in most normal adult tissues. It is thought that survivin enhances the survival of tumor cells primarily through the suppression of apoptosis-related cell death, which perhaps plays the role via direct inhibition of caspase-related proteins, and subsequently inhibits cell apoptosis. As shown in Figure 9, the results revealed the increased positive signals in the NS and mPEG-SAD micelle-treated tumors as compared to those in free DOX and mPEG-CAD-treated ones, indicating less cell apoptosis. The results indicated that mPEG-CAD micelle had downregulated the

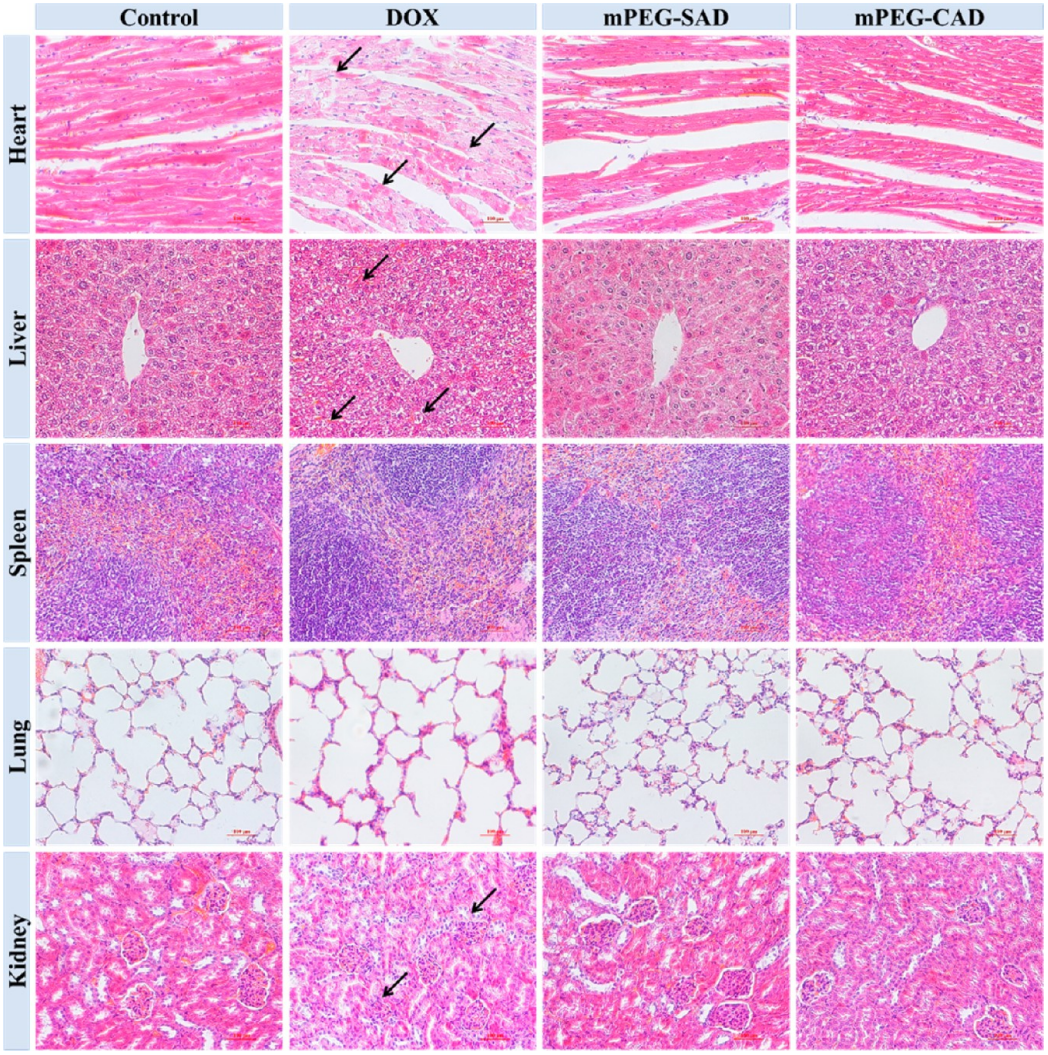

Figure 10. Histopathology analyses of visceral organ sections from H22-xenografted female Kunming mice after treatment with NS, free DOX, or mPEG-SAD or mPEG-CAD micelle. The arrows pointed out a certain myocardial damage and fracture, the blood oozing and nucleus shrunk of liver tissue, and nephrotoxicity judged from the shriveled glomerular and gathered nuclei. Magnification: 200×.

inhibitor of cell apoptosis in tumor tissue, which was consistent with the in vitro and in vivo antitumor results.

In summary, H&E, TUNEL, caspase-3, and survivin analyses all proved that mPEG-CAD micelles exhibited the highest suppression capability toward tumor growth as compared to free DOX and mPEG-SAD, which was consistent with the antitumor profiles in vitro and in vivo. These all indicated that mPEG-CAD exhibited great potential for application in clinical chemotherapy of malignancy.

3.5. In Vivo Security Evaluation. In clinical practice, most of antitumor drugs have serious side effects.[51] For example, DOX formulations always result in acute cardiactoxicity and nephrotoxicity.[20,21] Therefore, in vivo security of antitumor drugs is another critical evaluation index for clinical chemotherapy, which is directly linked to the survival of malignancy patients.[21]

In this study, the safety of prodrug micelles was systematically assessed through the detection of body weight change, histopathological analyses of internal organs (i.e., heart, liver, spleen, lung, and kidney), and quantitative evaluation of functional enzymes in serum.

For indicating the advantages of prodrug micelles in vivo, the body weight of the mouse was an important indicator of organism toxicity. All mice were alive in the whole process of the experiment. As shown in Figure 8B, a significant body weight loss was found in the free DOX group ascribed to the serious toxicity and side effects, while just a slight decrease of body weight was observed in mPEG-SAD and mPEG-CAD micelles groups in relation to that of NS group. The results revealed that the prodrug micelles exhibited improved safety in vivo.

Toxicity after long-term administration was an important indicator for in vivo application of chemotherapy, which can be analyzed by the immunohistochemistry of the main organ sections (e.g., heart, liver, spleen, lung, and kidney). In this work, as shown in Figure 10, free DOX group had a certain myocardial damage and fracture pointed out by arrows. However, in other groups, myocardial cells and nuclei were arranged in rules. The blood oozing and nucleus shrinking of liver tissue were pointed out by arrows. In addition, free DOX exhibited obvious nephrotoxicity judged from the shriveled glomerular and gathered nuclei noted by arrows. After modifying DOX with mPEG, the cardiotoxicity and nephrotox-

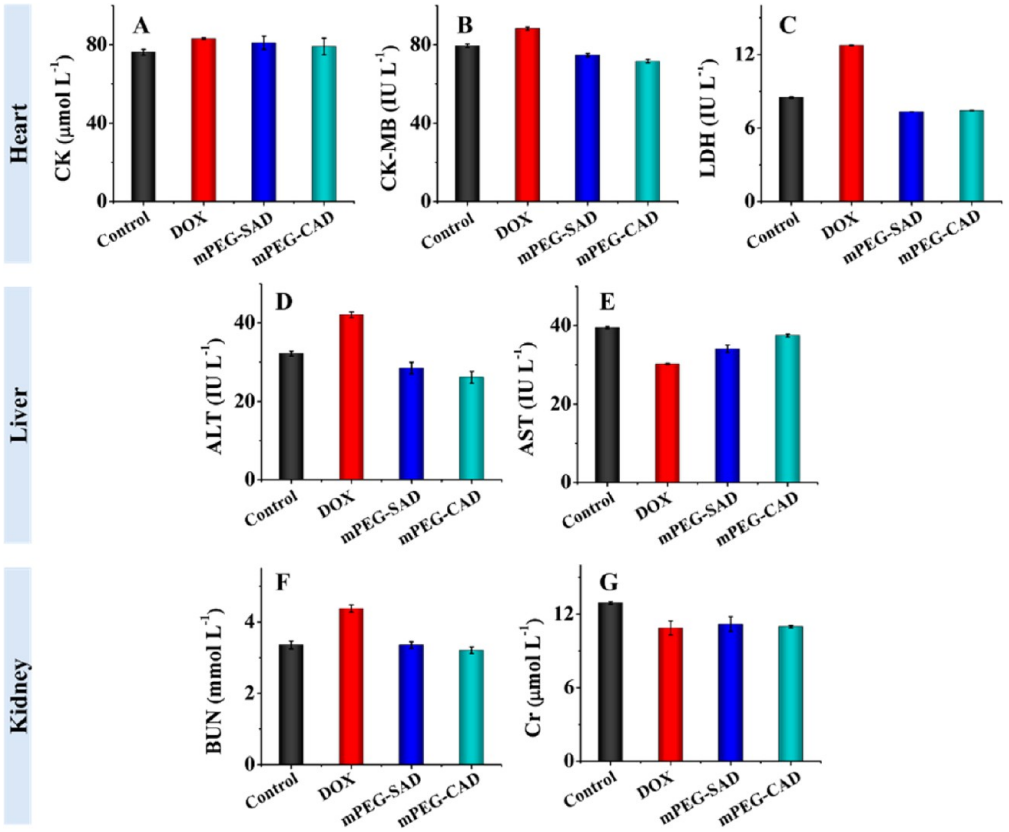

Figure 11. Evaluations of CK (A), CK-MB (B), LDH (C), ALT (D), AST (E), BUN (F), and Cr (G) after treatment with NS, free DOX, or mPEG-SAD or mPEG-CAD micelle. Magnification: 200×.

icity were significantly decreased. Furthermore, all DOX formulations exhibit no noticeable abnormal damages to spleen and lung.

To further verify whether prodrug micelles would cause damage to the normal organs, especially heart, liver, and kidney, some functional enzymes, that is, clinical chemical parameters, including heart indices containing CK, CK-MB, and LDH, liver-related ALT and AST, and kidney-associated BUN and Cr,[21] were evaluated by the commercial ELISA kits. As shown in Figure 11, all of the parameters of prodrug micelles groups remained at normal levels as control group, which proved that the treatments of mPEG-SAD and mPEG-CAD micelles did not cause obvious damage to the body. However, in the free DOX group, the heart, liver, and kidney parameters showed an obvious increase, which suggested that the treatment of free DOX caused some damage to heart, liver, and kidney. The results showed that the changes of functional enzyme were consistent with the changes of body weights and immunohistochemistry results of organs. All of the above data demonstrated that the prodrug micelles were secure to the body and could be potentially applied in clinic.

4. CONCLUSIONS

In this study, the insensitive mPEG-SAD and acid-sensitive mPEG-CAD with clear chemical structure were well-designed and facilely prepared for controlled DOX delivery. The prodrug micelles were prepared by direct dissolution approach with diameters at ∼100 nm, which was an appropriate scale for exhibited enhanced accumulation in tumor tissue through the EPR effect. mPEG-CAD micelle exhibit faster drug release in acidic PBS and intracellular microenvironment as compared to mPEG-SAD micelle. Moreover, mPEG-CAD micelle exhibited a higher in vitro antiproliferative activity than mPEG-SAD micelle and even free DOX after incubation for 72 h. In addition, mPEG-CAD micelle significantly inhibited H22 tumor growth in vivo due to the prolonged blood circulation time, enhanced accumulation at the tumor site, and increased intracellular DOX release. Even more unusual was that mPEG-CAD micelle exhibited almost no damage to the body. All positive data suggested that the acid-sensitive PEGylated DOX, that is, mPEG-CAD micelle, exhibited great potential for clinical chemotherapy of malignancy.

■ ASSOCIATED CONTENT

Supporting Information

Synthesis pathways for mPEG-SAD and mPEG-CAD, the serum-tolerance stability and hemocompatibility characterizations of prodrug micelles, and the relative necrotic areas of tumor sections after all treatments. This material is available free of charge via the Internet at http://pubs.acs.org.

■ AUTHOR INFORMATION

Corresponding Authors

*Tel.: +86 431 85262116. Fax: +86 431 85262116. E-mail: jxding@ciac.ac.cn.
*E-mail: zhuangxl@ciac.ac.cn.

Notes

The authors declare no competing financial interest.

■ ACKNOWLEDGMENTS

This work was financially supported by the National Natural Science Foundation of China (Projects 51303174, 51321062, 51233004, 51390484, 51273196, and 51203153) and the Scientific Development Program of Jilin Province (20140520050JH).

■ REFERENCES

(1) Shi, F.; Ding, J.; Xiao, C.; Zhuang, X.; He, C.; Chen, L.; Chen, X. Intracellular Microenvironment Responsive PEGylated Polypeptide Nanogels with Ionizable Cores for Efficient Doxorubicin Loading and Triggered Release. *J. Mater. Chem.* **2012**, *22*, 14168−14179.

(2) Chen, C. K.; Wang, Q.; Jones, C. H.; Yu, Y.; Zhang, H.; Law, W. C.; Lai, C. K.; Zeng, Q.; Prasad, P. N.; Pfeifer, B. A.; Cheng, C. Synthesis of pH-Responsive Chitosan Nanocapsules for the Controlled Delivery of Doxorubicin. *Langmuir* **2014**, *30*, 4111−4119.

(3) Xu, W.; Siddiqui, I. A.; Nihal, M.; Pilla, S.; Rosenthal, K.; Mukhtar, H.; Gong, S. Aptamer-Conjugated and Doxorubicin-Loaded Unimolecular Micelles for Targeted Therapy of Prostate Cancer. *Biomaterials* **2013**, *34*, 5244−5253.

(4) Ding, J.; Shi, F.; Li, D.; Chen, L.; Zhuang, X.; Chen, X. Enhanced Endocytosis of Acid-Sensitive Doxorubicin Derivatives with Intelligent Nanogel for Improved Security and Efficacy. *Biomater. Sci.* **2013**, *1*, 633−646.

(5) Felber, A. E.; Dufresne, M. H.; Leroux, J. C. pH-Sensitive Vesicles, Polymeric Micelles, and Nanospheres Prepared with Polycarboxylates. *Adv. Drug Delivery Rev.* **2012**, *64*, 979−992.

(6) Huang, Y.; He, L.; Liu, W.; Fan, C.; Zheng, W.; Wong, Y. S.; Chen, T. Selective Cellular Uptake and Induction of Apoptosis of Cancer-Targeted Selenium Nanoparticles. *Biomaterials* **2013**, *34*, 7106−7116.

(7) Liu, J.; Huang, Y.; Kumar, A.; Tan, A.; Jin, S.; Mozhi, A.; Liang, X. J. pH-Sensitive Nano-Systems for Drug Delivery in Cancer Therapy. *Biotechnol. Adv.* **2013**, *32*, 693−710.

(8) Koren, E.; Apte, A.; Jani, A.; Torchilin, V. P. Multifunctional PEGylated 2C5-Immunoliposomes Containing pH-Sensitive Bonds and TAT Peptide for Enhanced Tumor Cell Internalization and Cytotoxicity. *J. Controlled Release* **2012**, *160*, 264−273.

(9) Kluza, E.; Yeo, S. Y.; Schmid, S.; van der Schaft, D. W.; Boekhoven, R. W.; Schiffelers, R. M.; Storm, G.; Strijkers, G. J.; Nicolay, K. Anti-Tumor Activity of Liposomal Glucocorticoids: The Relevance of Liposome-Mediated Drug Delivery, Intratumoral Localization and Systemic Activity. *J. Controlled Release* **2011**, *151*, 10−17.

(10) Yuba, E.; Kojima, C.; Sakaguchi, N.; Harada, A.; Koiwai, K.; Kono, K. Gene Delivery to Dendritic Cells Mediated by Complexes of Lipoplexes and pH-Sensitive Fusogenic Polymer-Modified Liposomes. *J. Controlled Release* **2008**, *130*, 77−83.

(11) Sun, H.; Guo, B.; Cheng, R.; Meng, F.; Liu, H.; Zhong, Z. Biodegradable Micelles with Sheddable Poly(ethylene glycol) Shells for Triggered Intracellular Release of Doxorubicin. *Biomaterials* **2009**, *30*, 6358−6366.

(12) Liang, J.; Wu, W. L.; Xu, X. D.; Zhuo, R. X.; Zhang, X. Z. pH Responsive Micelle Self-Assembled from a New Amphiphilic Peptide as Anti-Tumor Drug Carrier. *Colloids Surf., B* **2014**, *114*, 398−403.

(13) Kim, Y.; Pourgholami, M. H.; Morris, D. L.; Stenzel, M. H. Triggering the Fast Release of Drugs from Crosslinked Micelles in an Acidic Environment. *J. Mater. Chem.* **2011**, *21*, 12777−12783.

(14) Das, M.; Mardyani, S.; Chan, W. C. W.; Kumacheva, E. Biofunctionalized pH-Responsive Microgels for Cancer Cell Targeting: Rational Design. *Adv. Mater.* **2006**, *18*, 80−83.

(15) Oh, J. K.; Lee, D. I.; Park, J. M. Biopolymer-Based Microgels/Nanogels for Drug Delivery Applications. *Prog. Polym. Sci.* **2009**, *34*, 1261−1282.

(16) Nukolova, N. V.; Oberoi, H. S.; Cohen, S. M.; Kabanov, A. V.; Bronich, T. K. Folate-Decorated Nanogels for Targeted Therapy of Ovarian Cancer. *Biomaterials* **2011**, *32*, 5417−5426.

(17) Barik, S.; Valiyaveettil, S. Synthesis and Self-Assembly of Polyhydroxylated and Electropolymerizable Block Copolymers. *J. Polym. Sci., Part A: Polym. Chem.* **2014**, *52*, 2217−2227.

(18) Gou, P.; Liu, W.; Mao, W.; Tang, J.; Shen, Y.; Sui, M. Self-Assembling Doxorubicin Prodrug Forming Nanoparticles for Cancer Chemotherapy: Synthesis and Anticancer Study *In Vitro* and *In Vivo*. *J. Mater. Chem. B* **2013**, *1*, 284−292.

(19) Markovsky, E.; Baabur-Cohen, H.; Satchi-Fainaro, R. Anticancer Polymeric Nanomedicine Bearing Synergistic Drug Combination Is Superior to a Mixture of Individually-Conjugated Drugs. *J. Controlled Release* **2014**, *187*, 145−157.

(20) Du, C.; Deng, D.; Shan, L.; Wan, S.; Cao, J.; Tian, J.; Achilefu, S.; Gu, Y. A pH-Sensitive Doxorubicin Prodrug Based on Folate-Conjugated BSA for Tumor-Targeted Drug Delivery. *Biomaterials* **2013**, *34*, 3087−3097.

(21) Ding, J.; Xu, W.; Zhang, Y.; Sun, D.; Xiao, C.; Liu, D.; Zhu, X.; Chen, X. Self-Reinforced Endocytoses of Smart Polypeptide Nanogels for "On-Demand" Drug Delivery. *J. Controlled Release* **2013**, *172*, 444−455.

(22) Yabbarov, N. G.; Posypanova, G. A.; Vorontsov, E. A.; Obydenny, S. I.; Severin, E. S. A New System for Targeted Delivery of Doxorubicin into Tumor Cells. *J. Controlled Release* **2013**, *168*, 135−141.

(23) Ibsen, S.; Zahavy, E.; Wrasdilo, W.; Berns, M.; Chan, M.; Esener, S. A Novel Doxorubicin Prodrug with Controllable Photolysis Activation for Cancer Chemotherapy. *Pharm. Res.* **2010**, *27*, 1848−1860.

(24) Zhou, T.; Xiao, C.; Fan, J.; Chen, S.; Shen, J.; Wu, W.; Zhou, S. A Nanogel of On-Site Tunable pH-Response for Efficient Anticancer Drug Delivery. *Acta Biomater.* **2013**, *9*, 4546−4557.

(25) Hu, F. Q.; Liu, L. N.; Du, Y. Z.; Yuan, H. Synthesis and Antitumor Activity of Doxorubicin Conjugated Stearic Acid-*g*-Chitosan Oligosaccharide Polymeric Micelles. *Biomaterials* **2009**, *30*, 6955−6963.

(26) Kamimura, M.; Furukawa, T.; Akiyama, S. I.; Nagasaki, Y. Enhanced Intracellular Drug Delivery of pH-Sensitive Doxorubicin/Poly(ethylene glycol)-*block*-Poly(4-vinylbenzylphosphonate) Nanoparticles in Multi-Drug Resistant Human Epidermoid KB Carcinoma Cells. *Biomater. Sci.* **2013**, *1*, 361−367.

(27) Wei, H.; Zhuo, R. X.; Zhang, X. Z. Design and Development of Polymeric Micelles with Cleavable Links for Intracellular Drug Delivery. *Prog. Polym. Sci.* **2013**, *38*, 503−535.

(28) Zelzer, M.; Todd, S. J.; Hirst, A. R.; McDonald, T. O.; Ulijn, R. V. Enzyme Responsive Materials: Design Strategies and Future Developments. *Biomater. Sci.* **2013**, *1*, 11−39.

(29) Thornton, P. D.; Mart, R. J.; Ulijn, R. V. Enzyme-Responsive Polymer Hydrogel Particles for Controlled Release. *Adv. Mater.* **2007**, *19*, 1252−1256.

(30) Ding, J.; Zhao, L.; Li, D.; Xiao, C.; Zhuang, X.; Chen, X. Thermo-Responsive "Hairy-Rod" Polypeptides for Smart Antitumor Drug Delivery. *Polym. Chem.* **2013**, *4*, 3345−3356.

(31) Calderon, M.; Quadir, M. A.; Strumia, M.; Haag, R. Functional Dendritic Polymer Architectures as Stimuli-Responsive Nanocarriers. *Biochimie* **2010**, *92*, 1242−1251.

(32) Li, J.; Yu, Z.; Jiang, H.; Zou, G.; Zhang, Q. Photo and pH Dual-Responsive Polydiacetylene Smart Nanocontainer. *Mater. Chem. Phys.* **2012**, *136*, 219−224.

(33) Chen, W.; Zhong, P.; Meng, F.; Cheng, R.; Deng, C.; Feijen, J.; Zhong, Z. Redox and pH-Responsive Degradable Micelles for Dually Activated Intracellular Anticancer Drug Release. *J. Controlled Release* **2013**, *169*, 171−179.

(34) Kamimura, M.; Kim, J. O.; Kabanov, A. V.; Bronich, T. K.; Nagasaki, Y. Block Ionomer Complexes of PEG-*block*-Poly(4-vinylbenzylphosphonate) and Cationic Surfactants as Highly Stable, pH Responsive Drug Delivery System. *J. Controlled Release* **2012**, *160*, 486−494.

(35) Lim, E. K.; Huh, Y. M.; Yang, J.; Lee, K.; Suh, J. S.; Haam, S. pH-Triggered Drug-Releasing Magnetic Nanoparticles for Cancer

Therapy Guided by Molecular Imaging by MRI. *Adv. Mater.* **2011**, *23*, 2436−2442.
(36) Savla, R.; Taratula, O.; Garbuzenko, O.; Minko, T. Tumor Targeted Quantum Dot-Mucin 1 Aptamer-Doxorubicin Conjugate for Imaging and Treatment of Cancer. *J. Controlled Release* **2011**, *153*, 16−22.
(37) Guan, X.; Li, Y.; Jiao, Z.; Chen, J.; Guo, Z.; Tian, H.; Chen, X. A pH-Sensitive Charge-Conversion System for Doxorubicin Delivery. *Acta Biomater.* **2013**, *9*, 7672−7678.
(38) Min, K. H.; Kim, J. H.; Bae, S. M.; Shin, H.; Kim, M. S.; Park, S.; Lee, H.; Park, R. W.; Kim, I. S.; Kim, K.; Kwon, I. C.; Jeong, S. Y.; Lee, D. S. Tumoral Acidic pH-Responsive MPEG-Poly(β-amino ester) Polymeric Micelles for Cancer Targeting Therapy. *J. Controlled Release* **2010**, *144*, 259−266.
(39) Ulbrich, K.; Etrych, T.; Chytil, P.; Pechar, M.; Jelinkova, M.; Rihova, B. Polymeric Anticancer Drugs with pH-Controlled Activation. *Int. J. Pharm.* **2004**, *277*, 63−72.
(40) Ding, X.; Liu, Y.; Li, J.; Luo, Z.; Hu, Y.; Zhang, B.; Liu, J.; Zhou, J.; Cai, K. Hydrazone-Bearing PMMA-Functionalized Magnetic Nanocubes as pH-Responsive Drug Carriers for Remotely Targeted Cancer Therapy *In Vitro* and *In Vivo*. *ACS Appl. Mater. Interfaces* **2014**, *6*, 7395−7407.
(41) He, H.; Chen, S.; Zhou, J.; Dou, Y.; Song, L.; Che, L.; Zhou, X.; Chen, X.; Jia, Y.; Zhang, J.; Li, S.; Li, X. Cyclodextrin-Derived pH-Responsive Nanoparticles for Delivery of Paclitaxel. *Biomaterials* **2013**, *34*, 5344−5358.
(42) Yabbarov, N. G.; Posypanova, G. A.; Vorontsov, E. A.; Popova, O. N.; Severin, E. S. Targeted Delivery of Doxorubicin: Drug Delivery System Based on PAMAM Dendrimers. *Biochemistry* **2013**, *78*, 884−894.
(43) Xin, Y.; Yuan, J. Schiff's Base as a Stimuli-Responsive Linker in Polymer Chemistry. *Polym. Chem.* **2012**, *3*, 3045−3055.
(44) Zhang, Z.; Chen, X.; Chen, L.; Yu, S.; Cao, Y.; He, C.; Chen, X. Intracellular pH-Sensitive PEG-*block*-Acetalated-Dextrans as Efficient Drug Delivery Platforms. *ACS Appl. Mater. Interfaces* **2013**, *5*, 10760−10766.
(45) Yang, X. Z.; Du, X. J.; Liu, Y.; Zhu, Y. H.; Liu, Y. Z.; Li, Y. P.; Wang, J. Rational Design of Polyion Complex Nanoparticles to Overcome Cisplatin Resistance in Cancer Therapy. *Adv. Mater.* **2014**, *26*, 931−936.
(46) Jiang, L.; Gao, Z. M.; Ye, L.; Zhang, A. Y.; Feng, Z. G. A pH-Sensitive Nano Drug Delivery System of Doxorubicin-Conjugated Amphiphilic Polyrotaxane-Based Block Copolymers. *Biomater. Sci.* **2013**, *1*, 1282−1291.
(47) Zhou, L.; Liang, D.; He, X.; Li, J.; Tan, H.; Li, J.; Fu, Q.; Gu, Q. The Degradation and Biocompatibility of pH-Sensitive Biodegradable Polyurethanes for Intracellular Multifunctional Antitumor Drug Delivery. *Biomaterials* **2012**, *33*, 2734−2745.
(48) Zhang, J. C.; Ding, J. X.; Xiao, C. S.; He, C. L.; Zhuang, X. L.; Yang, Y. N.; Chen, X. S. Synthesis and Characterization of Tumor-Acidity-Sensitive Poly (L-lysine)-Doxorubicin Conjugates. *Chem. J. Chin. Univ., Chin.* **2012**, *33*, 2809−2815.
(49) Dai, J.; Lin, S.; Cheng, D.; Zou, S.; Shuai, X. Interlayer-Crosslinked Micelle with Partially Hydrated Core Showing Reduction and pH Dual Sensitivity for Pinpointed Intracellular Drug Release. *Angew. Chem., Int. Ed.* **2011**, *50*, 9404−9408.
(50) Li, M.; Tang, Z.; Lv, S.; Song, W.; Hong, H.; Jing, X.; Zhang, Y.; Chen, X. Cisplatin Crosslinked pH-Sensitive Nanoparticles for Efficient Delivery of Doxorubicin. *Biomaterials* **2014**, *35*, 3851−3864.
(51) Ding, J.; Shi, F.; Xiao, C.; Lin, L.; Chen, L.; He, C.; Zhuang, X.; Chen, X. One-Step Preparation of Reduction-Responsive Poly(ethylene glycol)-Poly(amino acid)s Nanogels as Efficient Intracellular Drug Delivery Platforms. *Polym. Chem.* **2011**, *2*, 2857−2864.
(52) Zhou, K.; Wang, Y.; Huang, X.; Luby-Phelps, K.; Sumer, B. D.; Gao, J. Tunable, Ultrasensitive pH-Responsive Nanoparticles Targeting Specific Endocytic Organelles in Living Cells. *Angew. Chem., Int. Ed.* **2011**, *50*, 6109−6114.
(53) Sun, Y.; Zou, W.; Bian, S.; Huang, Y.; Tan, Y.; Liang, J.; Fan, Y.; Zhang, X. Bioreducible PAA-*g*-PEG Graft Micelles with High Doxorubicin Loading for Targeted Antitumor Effect Against Mouse Breast Carcinoma. *Biomaterials* **2013**, *34*, 6818−6828.
(54) Janicke, R. U. Caspase-3 Is Required for DNA Fragmentation and Morphological Changes Associated with Apoptosis. *J. Biol. Chem.* **1998**, *273*, 9357−9360.